Analysis of Ion-Temperature-Gradient Instabilities Using a Gyro-Fluid Model in Cylindrical Plasmas*)

Genryu HATTORI, Naohiro KASUYA[1)] and Masatoshi YAGI[2)]

Interdisciplinary Graduate School of Engineering Sciences, Kyushu University, 6-1 Kasuga-Koen, Kasuga, Fukuoka 816-8580, Japan

[1)]*Research Institute for Applied Mechanics, Kyushu University, 6-1 Kasuga-Koen, Kasuga, Fukuoka 816-8580, Japan*

[2)]*Japan Atomic Energy Agency, 2-166 Omotedate, Obuchi, Rokkasho-mura, Aomori 039-3212, Japan*

(Received 25 November 2014 / Accepted 2 March 2015)

The excitation condition for ion-temperature-gradient (ITG) instabilities in linear devices is investigated using a gyro-fluid equation. The finite-Larmor-radius effect is included in the model, which helps to stabilize ITG instabilities. The critical values of η, which is the ratio of the lengths of the density gradient to the temperature gradient, are obtained. Although the modenumbers of the most unstable modes are different with different discharge gases, their critical values have almost the same η level close to 1.0. The results are compared with those from the Hamaguchi–Horton model numerically and analytically.

Keywords: ion-temperature-gradient instability, finite-Larmor-radius effect, gyro-fluid equation, linear device

DOI: 10.1585/pfr.10.3401060

1. Introduction

Anomalous transport is one of the important issues in magnetic confined plasmas. Competition of several kinds of instabilities determines the formed turbulent structure, and the level of turbulent transport [1]. One of the causes for turbulent transport is an ion-temperature-gradient (ITG) driven microscopic instability (η_i mode) [2]. It has been predicted to be unstable when η_i (= $L_\mathrm{T}^{-1}/L_\mathrm{n}^{-1}$) exceeds some threshold, where the inverse of the density gradient length and the ion temperature gradient length are L_n^{-1} (= $-\mathrm{d}(\ln n_0)/\mathrm{d}r$) and L_T^{-1} (= $-\mathrm{d}(\ln T_0)/\mathrm{d}r$), respectively. Analyses of the ITG instability using fluid models and models including kinetic effects have been performed [3–5].

In experiments with high-temperature plasmas, it is difficult to identify the ITG instability because of the limited diagnostics available. Conversely, in laboratory plasmas using linear machines, detailed measurements of fluctuations can be conducted to identify the ITG instability [6]. In PANTA device [7], an ion sensitive probe and a laser induced fluorescence are used to measure temperature fluctuations. Furthermore, by employing phase tracking, nonlinear waveforms of fluctuations can be identified [8] to evaluate the heat flux. Numerical simulations for the linear growth rate of the ITG instability have also been investigated using the fluid model in PANTA, which shows that the mode with $k_\perp \rho_\mathrm{s} \sim O(1)$ is unstable even with a low ion temperature [9]. Here, $k_\perp$ and ρ_s are the wavenumber in the perpendicular direction and the effective Larmor radius, respectively. Therefore, it is necessary to include the finite-Larmor-radius (FLR) effect so as to perform a more quantitative analysis.

The target of this research is to clarify the excitation condition of ITG instabilities in the linear device PANTA. The ion Larmor radius is comparable to the plasma radius in linear devices, so we are developing a simulation code using a gyro-fluid model to include the FLR effect. By linearizing the model, the excitation condition of the ITG instability is evaluated. The local model is used for the first step. This paper is organized as follows. In the next section, the set of gyro-fluid equations is described. In Sec. 3, the excitation condition of the ITG instability is evaluated by local linear analyses. Comparison between the gyro-fluid and fluid model is performed in Sec. 4. The results are summarized in Sec. 5.

2. Model Equations

A set of gyro-fluid equations is derived by taking the moments of the following nonlinear electrostatic gyrokinetic equation in the velocity spaces [10]:

$$\frac{\partial F}{\partial t} + \nabla \cdot \left[F \left(v_{/\!/} \hat{b} + J_0 \boldsymbol{v}_\mathrm{E} \right) \right] - \frac{\partial}{\partial v_{/\!/}} \left(\frac{e}{m} F \hat{b} \cdot \nabla J_0 \Phi \right) = 0, \tag{1}$$

where F is the distribution function, $v_{/\!/}$ is the parallel velocity, $\hat{b}$ is the unit vector in the direction parallel to the magnetic field, $\boldsymbol{v}_\mathrm{E}$ is the $\boldsymbol{E} \times \boldsymbol{B}$ drift velocity, Φ is the electrostatic potential, and J_0 is a linear operator to perform gyro-averaging. The target plasma has a cylindrical configuration with a homogeneous magnetic field parallel to the axial direction, so the magnetic curvature terms can

author's e-mail: hattori@riam.kyushu-u.ac.jp

*) This article is based on the presentation at the 24th International Toki Conference (ITC24).

be eliminated. Applying gyro-kinetic ordering, the linear forms of the equations are as follows:

$$\frac{\mathrm{d}n}{\mathrm{d}t} + \nabla_{/\!/} n_{/\!/} \left(1 + \frac{\eta_{\mathrm{i}\perp}}{2}\hat{\nabla}_\perp^2\right)\frac{1}{L_\mathrm{n}}\frac{\partial \Psi}{r\partial\theta} = 0, \tag{2}$$

$$\frac{\mathrm{d}u_{/\!/}}{\mathrm{d}t} + \nabla_{/\!/}(n\tau_{/\!/} + T_{/\!/} + \Psi) = 0, \tag{3}$$

$$\frac{1}{\tau}\frac{\mathrm{d}T}{\mathrm{d}t} + \nabla_{/\!/}(2u + q) + \eta_{\mathrm{i}/\!/}\frac{1}{L_\mathrm{n}}\frac{\partial \Psi}{r\partial\theta} = -\frac{2\nu_{\mathrm{ii}}}{3\tau}(T_{/\!/} - T_\perp), \tag{4}$$

$$\frac{1}{\tau_\perp}\frac{\mathrm{d}T_\perp}{\mathrm{d}t} + \nabla_{/\!/} q_\perp \left[\frac{1}{2}\hat{\nabla}_\perp^2 + \eta_{\mathrm{i}\perp}\left(1 + \hat{\hat{\nabla}}^2\right)\right]\frac{1}{L_\mathrm{n}}\frac{\partial \Psi}{r\partial\theta} = \frac{\nu_{\mathrm{ii}}}{3\tau}(T_{/\!/} - T_\perp), \tag{5}$$

where n is the ion density, u is the ion velocity, Ψ is the gyro-averaged potential in which $\Psi \equiv \Gamma_0^{1/2}\Phi$ and $\tau = T/T_\mathrm{e}$, T is the ion temperature, T_e is the electron temperature, q is the heat flux, ν_{ii} is the collision frequency between the ions, and ρ_s is the effective Lamor radius evaluated from the electron temperature. The subscripts $/\!/$ and $\perp$ represent the quantities parallel and perpendicular to the direction of the magnetic field, respectively. Pade and $\langle J_0\rangle^2 = \Gamma_0$ approximations are applied, where

$$\Gamma_0^{1/2} = \frac{1}{\left(1 + \frac{b\tau_\perp}{2}\right)}, \tag{6}$$

$$b\tau_\perp = -\nabla_\perp^2 = \tau_\perp\left(k_r^2 + k_\theta^2\right). \tag{7}$$

Collisions are dominant in this system, and higher order moments of Eq. (1) give simplified forms of the heat flux as follows [11]:

$$q_{/\!/} = -\frac{3}{\nu_{\mathrm{ii}}\tau_\perp}\nabla_{/\!/} T_{/\!/}, \tag{8}$$

$$q_\perp = -\frac{1}{\nu_{\mathrm{ii}}\tau_\perp}\nabla_{/\!/} T_\perp. \tag{9}$$

The quasi-neutrality relation is given to be

$$\Gamma_0\left(n + \frac{1}{\tau_\perp}\frac{\nabla_\perp^2}{2}T_\perp\right) - (1 - \Gamma_0)\frac{\Psi}{\tau_\perp} = \Psi. \tag{10}$$

The FLR effect gives the difference between the local density and potential. Our gyro-fluid model consists of Eqs. (2 - 5) and (10). The FLR effect is included in Ψ, $\hat{\nabla}_\perp^2$ and $\hat{\hat{\nabla}}^2$ terms, where

$$\frac{\hat{\nabla}_\perp^2}{2}\Psi \equiv -\frac{\frac{b\tau_\perp}{2}}{\left(1 + \frac{b\tau_\perp}{2}\right)}\Psi, \tag{11}$$

$$\hat{\hat{\nabla}}^2\Psi \equiv \frac{\frac{b\tau_\perp}{2}\left(\frac{b\tau_\perp}{2} - 1\right)}{\left(1 + \frac{b\tau_\perp}{2}\right)^2}\Psi. \tag{12}$$

The following normalizations are used:

$$r/\rho_\mathrm{s} \to r, \tag{13}$$

$$\Omega_{\mathrm{ci}}t \to t, \tag{14}$$

$$\left(\frac{n_1}{n_0}, \frac{u_{/\!/}}{c_\mathrm{s}}, \frac{T_{/\!/1}}{T_\mathrm{e}}, \frac{T_{\perp 1}}{T_\mathrm{e}}, \frac{q_{/\!/1}}{n_0 T_{/\!/0} c_\mathrm{s}}, \frac{q_{\perp 1}}{n_0 T_{\perp 0} c_\mathrm{s}}, \frac{e\Psi}{T_\mathrm{e}}\right) \to (n, u_{/\!/}, T_{/\!/}, T_\perp, q_{/\!/}, q_\perp, \Psi), \tag{15}$$

where $\Omega_{\mathrm{ci}} = eB/m_\mathrm{i}$ is the ion cyclotron frequency, $c_\mathrm{s} = \Omega_{\mathrm{ci}}\rho_\mathrm{s}$ is the ion sound velocity, and the subscripts 0 and 1 denote the equilibrium and fluctuating component, respectively.

3. Linear Growthrate Analysis

Local linear analyses are conducted to evaluate the excitation condition of the ITG instability. To linearize the set of equations, the differential operators d/dt, $\nabla_{/\!/}$ and $\nabla_\perp$ are replaced by λ, ik_z, and $ik_\perp$, where the real and imaginary part of λ are the growthrate and frequency, k_z and $k_\perp$ are the wavenumber in the parallel and perpendicular direction, respectively. This is a local model, so the results are basically the same as those with a slab geometry. The size of the plasma is reflected in the values of the mode numbers. The axial mode number is assumed to be 1, which gives $k_z = 2\pi/l$, where l is the device length. The radial and azimuthal wavenumbers are assumed to be the same ($k_r = k_\theta$), which gives $k_\perp^2 = 2k_\theta^2 = 2(m/r)^2$, where m is the poloidal mode number. The radial wavelength is approximately $2a$ for the fundamental ITG modes [9], so this assumption is used. This is a simplification for qualitative understanding, and the global mode analysis including the radial structure will be considered in future work. For linear analysis, experimental parameters in PANTA are used: $l = 4.0$ m, plasma radius $a = 7.0$ cm, density $n = 1.0\times10^{19}$ m^{-3}, $L_\mathrm{n} = 7.0$ cm, $\nu_{\mathrm{ii}} = 350$ s^{-1}, magnetic field $B = 0.1$ T, which gives $\Omega_{\mathrm{ci}}/2\pi = 1.5$ MHz. Temperatures $T_\mathrm{e} = 3$ eV and $T_\mathrm{i} = 0.3$ eV give $\rho_\mathrm{s} = 1.1$ cm and $\rho_\mathrm{i} = 3.5$ mm. With these parameters, $\rho_\mathrm{i}/L_\mathrm{n} = 0.05 \ll 1.0$, $k_z\rho_\mathrm{i} = 5.5\times10^{-3} \ll 1.0$ and $k_\perp\rho_\mathrm{i} = 0.02 \ll 1.0$, so gyro-kinetic ordering is satisfied. The other parameters for the analysis are τ and η_i, which correspond to the ratios between ions and electrons. Here, linear growthrates at $r = a/2$ are calculated.

First, the excitation conditions with different discharge gases are analyzed. In Fig. 1, the ion mass dependences of critical η_c of the modes with $m = 1$ - 5 are shown. The cases of helium, neon, and argon are plotted. The minimum values of η_c are close to 1 even though the ion mass numbers are different. This result suggests that there is no preferential gas for the ITG excitation. However, mode-numbers of most unstable modes depend on the discharge gasses (He: $m = 5$, Ne and Ar: $m = 2$), so the azimuthal mode structure can be different for fluctuations.

Next, temperature dependence and its gradient length are evaluated. In Fig. 2, a contour plot of the growth rate in the τ and η space, assuming $\eta_{/\!/} = \eta_\perp$ ($= \eta$) and $\tau_{/\!/} = \tau_\perp$ ($= \tau$) is shown. The critical value η_c for the ITG instability

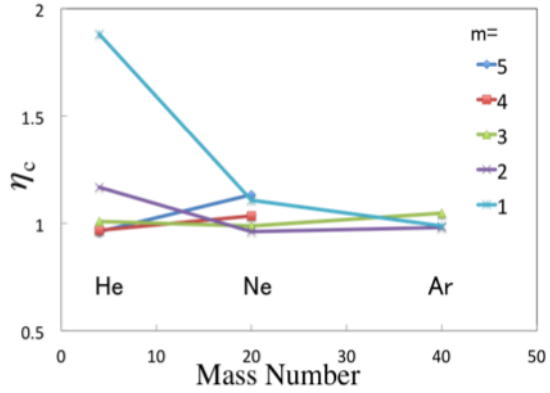

Fig. 1 Ion mass dependences of critical η_c, when $\tau = 1$. Those of modes with $m = 1$ - 5 are plotted.

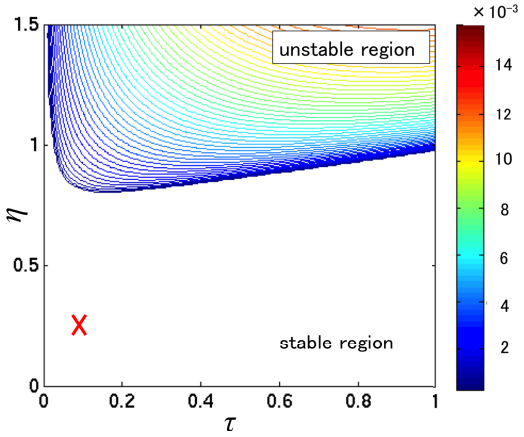

Fig. 2 Contour plot of the growth rate in the τ and η space. The boundary for unstable ITG mode is shown. The cross represents one set of experimental conditions in PANTA.

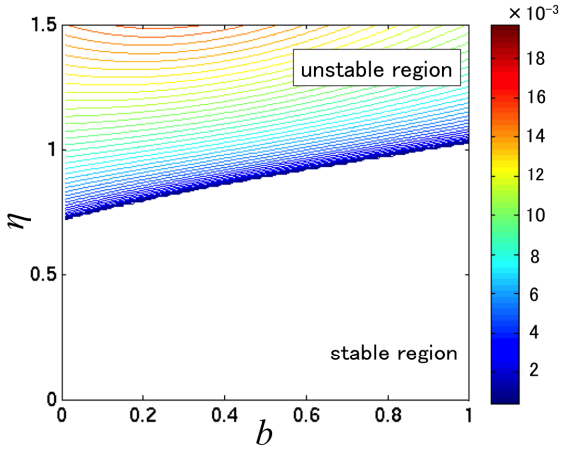

Fig. 3 Contour plot of the growth rate in the b and η space. This is the case with $\tau = 1.0$ of argon plasma.

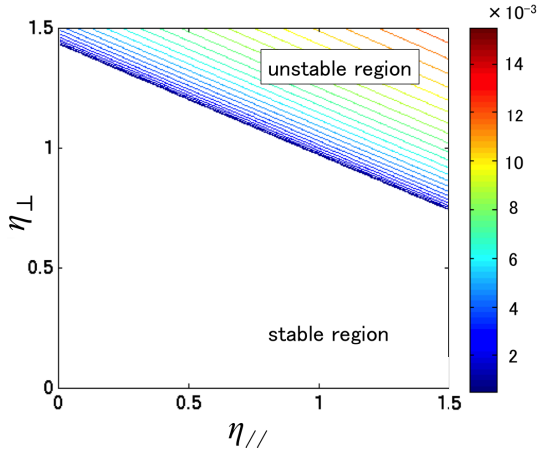

Fig. 4 Contour plot of the growthrate in the $\eta_{//}$ and $\eta_\perp$ space. This is the case with $\tau = 1.0$ of argon plasma.

changes depending on the magnitude of τ. The minimum $\eta_c = 0.81$ is given with $\tau = 0.15$, and η_c increases as τ increases (e.g., $\eta_c = 0.98$, when $\tau = 1.0$). When τ is low ($\tau \ll 0.15$), η_c is large and the ITG mode is rarely unstable. The cross in Fig. 2 indicates one set of experimental conditions in PANTA ($\tau = 0.1$, $\eta = 0.2$ with argon discharge). It suggests that a larger temperature gradient is needed to observe the excitation of the ITG mode in PANTA.

Characteristic dependencies of the threshold value are evaluated next. Our model includes the FLR effect, which depends on the magnitude of variable b, so the FLR effect is investigated by varying b. In Fig. 3, a contour plot of the growthrate in the b and η space is shown. The critical η_c increases with b, so the FLR effect stabilizes the ITG mode. Notes that the PANTA parameter gives $b = 0.8$. In addition, our model contains a thermal anisotropy as in Eqs. (4) and (5), so the anisotropic case with $\eta_{//} \neq \eta_\perp$ can be analyzed. In Fig. 4, a contour plot of the growthrate in the $\eta_{//}$ and $\eta_\perp$ space is shown. Fitting the critical boundary to the linear equation $\alpha\eta_\perp + \eta_{//} = \text{Const}$ gives $\alpha = 2.1 \pm 0.1$. The degree of freedom is 2 in the perpendicular direction, which corresponds to the obtained α value.

4. Comparison of the Gyro-Fluid and Fluid Model

We have used the gyro-fluid model to evaluate the ITG excitation condition in PANTA. Conversely, the ITG analyses have been conducted using the Hamaguchi–Horton (H–H) model, which consists of fluid equations [12, 13]. The results from the H–H model show that the critical temperature gradient is smaller than that with the gyro-fluid model. Comparison between these two models is shown in this section.

The H–H model solves three fields with the ion continuity equation, momentum conservation equation, and energy conservation equation:

$$\frac{\partial}{\partial t}\left[1 - \nabla_\perp^2\right]\phi + \nabla_{//}u_{//} + \frac{1}{L_n}\frac{\partial\phi}{r\partial\theta} + \tau\frac{1}{L_P}\frac{\partial}{r\partial\theta}\left(\nabla_\perp^2\phi\right) = 0, \quad (16)$$

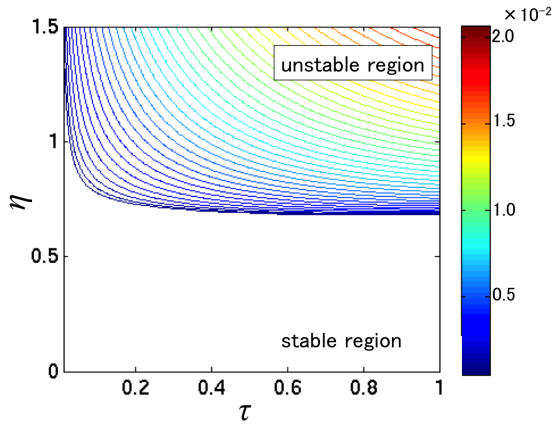

Fig. 5 Contour plot of the growthrate in the τ and η space with the H–H model. This is the case of argon plasma.

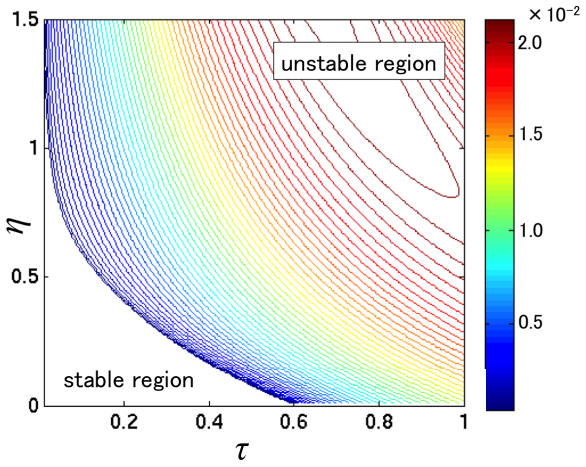

Fig. 6 Contour plot of the growthrate in the τ and η space with the reduced gyro-fluid model. This is the case of argon plasma.

$$\frac{\partial u_{//}}{\partial t} + \nabla_{//}(\phi + P) = 0, \tag{17}$$

$$\frac{\partial P}{\partial t} + \gamma\tau\nabla_{//}u_{//} + \tau\frac{1}{L_{\rm P}}\frac{\partial\phi}{r\partial\theta} = 0, \tag{18}$$

where P is the ion pressure. For comparison, a reduced set of the gyro-fluid model equations is obtained with isotropic temperature $T_{//} = T_{\perp} = T$ as

$$\frac{\partial}{\partial t}\left[1 - \left(1 + \frac{1}{\tau}\nabla_{\perp}^2\right)\right]\phi + \nabla_{//}u_{//} + \frac{1}{L_{\rm n}}\frac{\partial\phi}{r\partial\theta} + \frac{1}{2}\frac{1}{L_{\rm T}}\frac{\partial}{r\partial\theta}(\nabla_{\perp}^2\phi) = 0, \tag{19}$$

$$\frac{\partial u_{//}}{\partial t} + \left[1 + \tau + b\tau\left(1 + \frac{1}{\tau}\right)\right]\nabla_{//}\phi + \left(1 + \frac{b\tau}{2}\right)\nabla_{//}T = 0, \tag{20}$$

$$\frac{\partial T}{\partial t} + \frac{2}{3}\tau\nabla_{//}u_{//} + \tau\frac{1}{L_{\rm T}}\frac{\partial\phi}{r\partial\theta} = 0. \tag{21}$$

Here, the heat-flux terms and the FLR terms in Eqs. (2 - 5) are neglected, and the FLR term with variable b is only retained in the quasi-neutrality relation given in Eq. (10). Equation (21) is obtained by adding Eqs. (4) and (5). The basic frameworks of the two sets of the models are similar, though some of the coefficients are different.

In Figs. 5 and 6, contour plots of the growthrate in the τ and η space with the H–H model and the reduced gyro-fluid model, respectively, are given. Critical $\eta_{\rm c}$ is much smaller in the case with the H–H model than with the gyro-fluid model. In Fig. 5 the mode is unstable even with $\eta = 0$, when τ is greater than 0.6. Figure 6 shows the same level of critical $\eta_{\rm c}$ as in Fig. 1 even with this reduced set of equations, although the dependency on τ becomes weaker.

The results differ because of the different origins of the term in each model, i.e., the polarization velocity term in the H–H model, and the gyro-averaging in the gyro-fluid model. In the H–H model, the polarization term can couple with the diamagnetic drift term, which is not included in the gyro-fluid model. When $\omega \ll \omega_*$, the analytical solutions become

$$\omega = \pm k_z\sqrt{\frac{\tau(1+\eta)}{1 - b\tau(1+\eta)} - \gamma\tau}, \tag{22}$$

with the H–H model, and

$$\omega = \pm k_z\sqrt{\left(1 + \frac{b\tau}{2}\right)\left(\frac{\tau\eta}{1 - b\tau\eta/2} - \frac{2}{3}\tau\right)}, \tag{23}$$

with the reduced gyro-fluid model, where $\omega_* = k_\theta/L_{\rm n}$ is the diamagnetic drift frequency. Critical $\eta_{\rm c}$ is obtained to be

$$\eta_{\rm c} = \frac{\gamma}{1 + \gamma b\tau} - 1, \tag{24}$$

with the H–H model, and

$$\eta_{\rm c} = \frac{2}{3 + b\tau}, \tag{25}$$

with the reduced gyro-fluid model. By setting $b = 0$ and using $\gamma = 5/3$, the condition for ITG excitation $\eta > 2/3$ can be derived from both models.

5. Summary

The excitation condition for the ITG instability in linear device PANTA has been investigated using the gyro-fluid model. Linear stability analyses show the dependencies of the linear growthrate on the ion mass, the temperature gradient, the magnitude of the FLR effect, and the thermal anisotropy. Although the modenumbers of the most unstable modes differ for different discharge gases, their critical values have almost the same η value, i.e., ~1.0. The results from the gyro-fluid model and the H–H model differ owing to the origin of the $\nabla_{\perp}$ terms. From the gyro-fluid model, η is needed to be four times larger in order to observe the ITG instability in PANTA.

Acknowledgements

Authors acknowledge discussions with Prof. S. Inagaki, Dr. M. Sasaki, Dr. Y. Kosuga, and Mr. Y. Miwa. This work is supported by the Grant-in-Aid for Young Scientists (24760703), for Scientific Research (23244113) of JSPS, by the collaboration program of NIFS (NIFS13KNST050, NIFS13KOCT001) and of RIAM of Kyushu University.

[1] P.H. Diamond *et al.*, Plasma Phys. Control. Fusion **47**, R35 (2005).
[2] W. Horton, Rev. Mod. Phys. **71**, 735 (1999).
[3] B. Coppi *et al.*, Phys. Fluids **10**, 582 (1967).
[4] G.W. Hammett and F.W. Perkins, Phys. Rev. Lett. **64**, 3019 (1990).
[5] G.S. Lee and P.H. Diamond, Phys. Fluids **29**, 3291 (1986).
[6] A.K. Sen *et al.*, Phys. Rev. Lett. **66**, 429 (1991).
[7] S. Oldenbürger *et al.*, Plasma Phys. Control. Fusion **54**, 055002 (2012).
[8] S. Inagaki *et al*., Plasma Fusion Res. **9**, 1201216 (2014).
[9] Y. Miwa *et al.*, Plasma Fusion Res. **8**, 2403133 (2013).
[10] W. Dorland and G.W. Hammett, Phys. Fluids B **5**, 812 (1993).
[11] P. Snyder, Ph. D. thesis, Princeton Univ. (1999).
[12] S. Hamaguchi and W. Horton, Phys. Fluids B **2**, 1833 (1990).
[13] R. Balescu, *Aspect of Anomalous Transport in Plasmas* (CRC Press, 2005).